Molecular Therapy
Nucleic Acids
Original Article

Two antisense RNAs—AFAP1-AS1 and MLK7-AS1—promote colorectal cancer progression by sponging miR-149-5p and miR-485-5p

Tae Won Kim,[1,5] Haein Ji,[1,5] Nak Hyeon Yun,[1] Chang Hoon Shin,[1] Hyeon Ho Kim,[1,2] and Yong Beom Cho[1,3,4]

[1]Department of Health Sciences and Technology, Samsung Advanced Institute for Health Sciences and Technology, Sungkyunkwan University, Seoul 06351, Republic of Korea; [2]Institute for Future Medicine, Samsung Medical Center, Seoul 06351, Republic of Korea; [3]Department of Surgery, Samsung Medical Center, Sungkyunkwan University School of Medicine, Seoul 06351, Republic of Korea; [4]Department of Biopharmaceutical Convergence, Sungkyunkwan University, Gyeonggi-do 16419, Republic of Korea

Colorectal cancer (CRC) is one of the leading causes of cancer-related deaths. Antisense RNAs (asRNAs) are closely associated with cancer malignancy. This study aimed to identify the action mechanism of asRNAs in controlling CRC malignancy. Analysis of the RNA sequencing data revealed that AFAP1-AS1 and MLK7-AS1 were upregulated in CRC patients and cell lines. High levels of both asRNAs were associated with poor prognosis in patients with CRC. Both *in vitro* and *in vivo* experiments revealed that the knockdown of the two asRNAs decreased the proliferative and metastatic abilities of CRC cells. Mechanistically, AFAP1-AS1 and MLK7-AS1 decreased the levels of miR-149-5p and miR-485-5p by functioning as ceRNAs. Overexpression of miRNAs by introducing miRNA mimics suppressed the expression of *SHMT2* and *IGFBP5* by directly binding to the 3′ UTR of their mRNA. Knockdown of both asRNAs decreased the expression of SHMT2 and IGFBP5, which was reversed by inhibition of both miRNAs by miRNA inhibitors. *In vivo* pharmacological targeting of both asRNAs by small interfering RNA-loaded nanoparticles showed that knockdown of asRNAs significantly reduced tumor growth and metastasis. Our findings demonstrate that AFAP1-AS1 and MLK7-AS1 promote CRC progression by sponging the tumor-suppressing miRNAs miR-149-5p and miR-485-5p, thus upregulating SHMT2 and IGFBP5.

INTRODUCTION

Colorectal cancer (CRC) is a commonly diagnosed cancer worldwide and one of the leading causes of cancer-related deaths.[1,2] Despite the high mortality, no effective treatment has yet been developed.[3] The poor prognosis in patients with CRC is due to the occurrence of metastasis.[4] The 5-year survival rate for CRC is approximately 64%, whereas the survival rate for metastatic CRC has decreased to 12%.[4] Although various treatments for CRC including combination chemotherapy with 5-fluorouracil, irinotecan, oxaliplatin, and antiangiogenetic or epidermal growth factor receptor-directed drugs have been developed, the therapeutic effect on metastatic colon cancer is very limited. Accordingly, our research goal was to develop an effective treatment for CRC based on a network of non-coding RNAs (ncRNAs).

Approximately 90% of the human genome is transcribed into RNA. However, only 2% of the genome comprises protein-coding genes.[5] Moreover, ncRNAs are known to regulate essential biological processes and are closely associated with many human diseases, particularly cancer.[6,7] Recently, ncRNAs were reported to act as competing endogenous RNAs (ceRNAs) by directly binding to microRNAs (miRNAs) through shared miRNA response elements (MREs).[8] Thus, antisense RNAs (asRNAs) mitigate the inhibitory function of miRNAs and upregulate the target genes of decoying miRNAs.[9] Recently, the functional role of ceRNAs in cancer malignancy has attracted considerable attention for the development of new cancer treatments.[10] Several studies showed that asRNAs promote CRC progression by sponging tumor-suppressing miRNAs in CRC.[11–13] NNT-AS1 regulates proliferation, migration, and invasion via the miR-496/RAP2C axis in CRC.[11] CERS6-AS1 promotes the proliferation, migration, invasion, epithelial-mesenchymal transition (EMT), and stemness of CRC cells by binding to miR-15b-5p to upregulate SPTBN2.[12] Furthermore, OIP5-AS1 regulates drug resistance by abolishing the miR-137-mediated suppression of DYRK1A in CRC.[13]

We discovered two oncogenic asRNAs—AFAP1-AS1 and MLK7-AS1—whose expression levels were higher in CRC than in normal tissues and showed promise as candidates for CRC treatment. Knockdown of each or both asRNAs represses malignant phenotypes such

Received 1 December 2022; accepted 11 July 2023;
https://doi.org/10.1016/j.omtn.2023.07.004.

[5]These authors contributed equally

Correspondence: Hyeon Ho Kim, Department of Health Sciences and Technology, Samsung Advanced Institute for Health Sciences and Technology, Sungkyunkwan University, Seoul 06351, Republic of Korea.
E-mail: hyeonhkim@skku.edu
Correspondence: Yong Beom Cho, Department of Health Sciences and Technology, Samsung Advanced Institute for Health Sciences and Technology, Sungkyunkwan University, Seoul 06351, Republic of Korea.
E-mail: gscyb@skku.edu

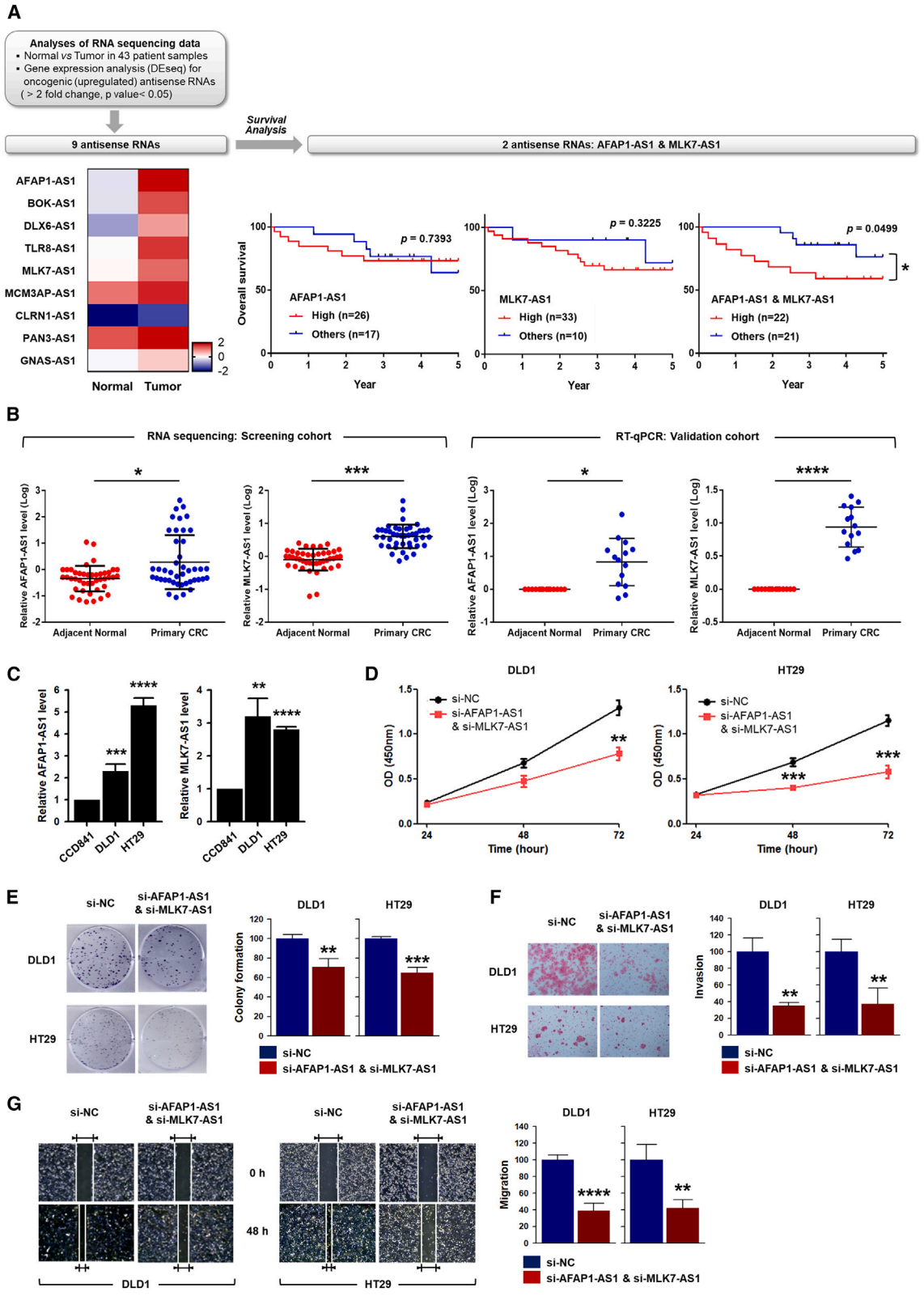

(legend on next page)

as proliferation, colony formation, migration, and invasion. Mechanistically, we revealed that both asRNAs functioned as ceRNAs of tumor-suppressing miR-149-5p and miR-485-5p and mitigated their inhibitory function, which increased the expression of their common targets, *SHMT2* and *IGFBP5*. In addition, the therapeutic potential of AFAP1-AS1 and MLK7-AS1 was identified by examining the tumor-suppressing effects, such as tumor growth and metastasis, of nanoparticles loaded with asRNA-targeting small interfering RNAs (siRNAs) on CRC.

RESULTS

AFAP1-AS1 and MLK7-AS1 are highly expressed in CRC tissues than in normal tissues

To identify differentially expressed asRNAs in CRC, we performed RNA sequencing using 43 samples isolated from tumors and matched normal tissues of patients with CRC. Overall, two asRNAs were selected according to the workflow shown in Figure 1A. By analyzing the RNA sequencing data, nine upregulated asRNAs were identified (fold change >2, $p < 0.05$) (Figure 1A). To investigate the clinical outcomes of the nine asRNAs in patients with CRC, survival analysis was conducted in our cohort. Among the nine upregulated asRNAs, only AFAP1-AS1 and MLK7-AS1 were validated and showed association with poor prognosis. MCM3AP-AS1 was associated with poor prognosis, but MCM3AP-AS1 was not selected because inhibition of metastatic potential including migratory and invasive abilities was not observed in MCM3AP-AS1-silenced DLD1 cells (Figure S1). No statistically significant correlation existed between any of the asRNAs and prognosis of CRC patients, except when the expression of both asRNAs was high. CRC patients with high levels of both AFAP1-AS1 and MLK7-AS1 showed poor prognosis compared with those with lower expression levels. Therefore, we decided to investigate the role of AFAP1-AS1 and MLK7-AS1 in the acquisition of malignant phenotypes in CRC.

RNA sequencing data analysis indicated that the expression levels of AFAP1-AS1 and MLK7-AS1 were higher in primary CRC tissues than in the adjacent normal tissues (Figure 1B, left). Similarly, the qRT-PCR assay in the validation cohort showed that the two asRNAs were upregulated in primary CRC tissues compared with their expression in the matched normal samples ($n = 14$; Figure 1B, right). Collectively, we hypothesized that AFAP1-AS1 and MLK7-AS1 are upregulated in CRC and are closely associated with CRC progression. As a result of determining the expression levels of asRNAs in CRC cell lines, we found that both AFAP1-AS1 and MLK7-AS1 expression was higher in DLD1 and HT29 cells than in the normal epithelial cell line CCD841 (Figure 1C). Therefore, we used both CRC cell lines, DLD1 and HT29, to evaluate the function of AFAP1-AS1 and MLK7-AS1.

Knockdown of AFAP1-AS1 and MLK7-AS1 suppressed proliferative ability

To investigate the role of AFAP1-AS1 and MLK7-AS1 in the proliferation of CRC cells, DLD1 and HT29 cells were transfected with three different siRNAs targeting AFAP1-AS1 and MLK7-AS1 (designated si-AFAP1-AS1#1–3 and si-MLK7-AS1#1–3). All the siRNAs efficiently decreased the asRNA levels (Figure S2A for AFAP1-AS1 siRNA and Figure S2B for MLK7-AS1 siRNA) and none of siRNAs affect the expression of the other asRNA (Figure S2C). The WST-1 cell proliferation assay indicated that the knockdown of either AFAP1-AS1 or MLK7-AS1 reduced the proliferation of DLD1 and HT29 cells (Figure S3A). Moreover, when the expression of both AFAP1-AS1 and MLK7-AS1 was reduced by the siRNA mixture, the proliferation of DLD1 and HT29 cells was significantly suppressed (Figure 1D).

The colony-forming assay also revealed that knockdown of AFAP1-AS1 or MLK7-AS1 by all the tested siRNAs decreased the number of colonies (Figure 1E for both siRNAs, Figure S3B for AFAP1-AS1, and Figure S3C for MLK7-AS1). These results demonstrated that the two selected asRNAs, AFAP1-AS1 and MLK7-AS1, are closely associated with CRC proliferation.

Knockdown of AFAP1-AS1 and MLK7-AS1 inhibited metastatic potential

To further determine whether an association existed between AFAP1-AS1 and MLK7-AS1 and the metastatic potential in CRC, we examined whether knockdown of AFAP1-AS1 and MLK7-AS1 suppressed the invasion and migration of DLD1 and HT29 cells. The transwell assay indicated that the number of invading cells was decreased among the AFAP1-AS1- and MLK7-AS1-silenced DLD1 and HT29 cells (Figure S4A for AFAP1-AS1 and Figure S4B for MLK7-AS1). In addition, the invasive abilities of both cells were significantly reduced by the simultaneous knockdown of AFAP1-AS1 and MLK7-AS1 (Figure 1F). The wound healing assay showed that knockdown of AFAP1-AS1 or MLK7-AS1 inhibited the mobility of DLD1 and HT29 cells (Figure S4C for AFAP1-AS1 and Figure S4D for MLK7-AS1), implying reduced invasiveness. As expected, simultaneous knockdown of AFAP1-AS1 and MLK7-AS1 significantly inhibited cell migration compared with the knockdown of each asRNA individually (Figure 1G).

Figure 1. AFAP1-AS1 and MLK7-AS1 were upregulated and required for malignant phenotypes of CRC

(A) Schematic workflow for screening differentially expressed antisense RNAs (asRNAs) and the association of AFAP1-AS1 and MLK7-AS1 with the prognosis of patients with CRC. More than 2-fold high expression was classified as "High," and all others were classified as "Others" to analyze the prognosis. (B) Analysis of RNA sequencing data (left) and validation (right, $n = 14$) by qRT-PCR proving the higher levels of AFAP1-AS1 and MLK7-AS1 in CRC tissues compared with that in adjacent normal tissues. (C) The expression levels of AFAP1-AS1 and MLK7-AS1 in normal colonic epithelial cells (CCD841) and two CRC cells (DLD1 and HT29) were determined by qRT-PCR. (D–G) After DLD1 and HT29 cells were transfected with small interfering RNAs (siRNAs) targeting AFAP1-AS1/MLK7-AS1, cell proliferation was assessed by WST-1 (D) and colony-forming assay (E). Invasive and migratory abilities were determined by transwell (F) and wound healing assay (G).

Data are expressed as mean ± standard deviation. Statistical significance was set at $p < 0.05$ (*$p < 0.05$, **$p < 0.01$, ***$p < 0.001$, or ****$p < 0.0001$).

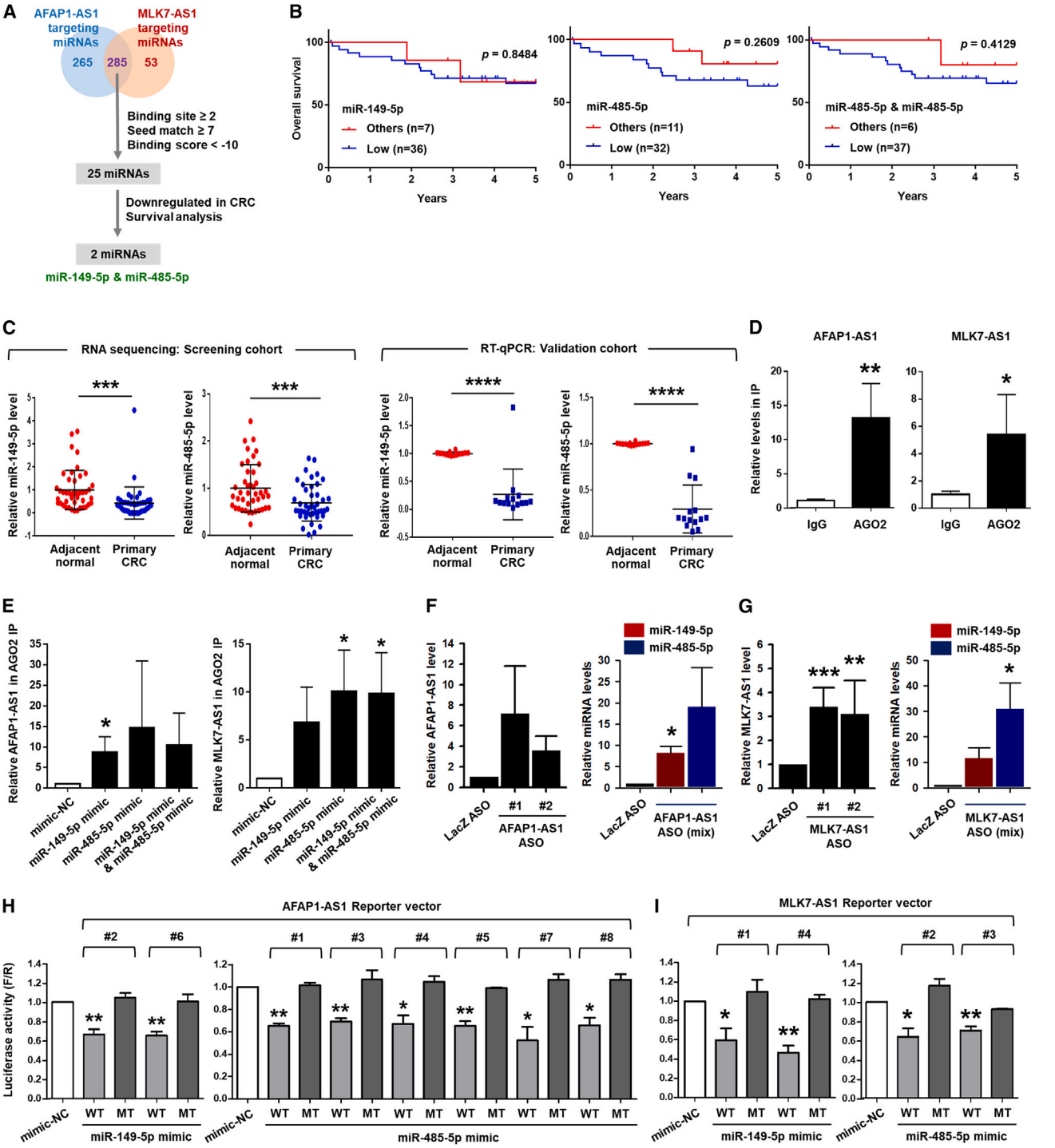

Figure 2. AFAP1-AS1 and MLK7-AS1 function as a ceRNA for miR-149-5p and miR-485-5p

(A) Schematic workflow for selecting AFAP1-AS1/MLK7-AS1-associated miRNAs: miR-149-5p and miR-485-5p. Detailed information on the criteria has been described in main text. (B) Kaplan-Meier overall survival curves of patients with CRC with both low and high levels of miR-149-5p and/or miR-485-5p. Less than 2-fold low expression was classified as "Low," and all others were classified as "Others" to analyze the prognosis. (C) RNA sequencing data representing lower expression of miR-149-5p and/or miR-485-5p in CRC compared with that in adjacent normal tissues. (D) The enrichment of AFAP1-AS1 and MLK7-AS1 was examined by performing AGO2 ribonucleoprotein immunoprecipitation (AGO2 RIP) experiment. The levels of AFAP1-AS1 and MLK7-AS1 in AGO2 IP were determined by qRT-PCR. (E) After overexpression of miR-149-5p

(legend continued on next page)

Given the correlation between CRC patient prognosis and the inhibitory effects on cell proliferation and metastatic potential, a more definite tumor-suppressing effect was observed when both asRNAs were silenced simultaneously than when the levels of each asRNA were decreased separately (Figure S5). Accordingly, further studies were conducted with focus on the regulatory mechanisms coregulated by AFAP1-AS1 and MLK7-AS1.

AFAP1-AS1 and MLK7-AS1 sponge miRNA-149-5p and miRNA-485-5p

Accumulating evidence has revealed that long non-coding (lncRNAs), including asRNAs, directly interact with miRNAs and weaken their inhibitory effects on the expression of their target genes. Therefore, a prediction software was used to predict the potential miRNA candidates associated with AFAP1-AS1 and MLK7-AS1. More reliable miRNA candidates that bound to both asRNAs were selected by applying three criteria: (1) more than two MREs in the sequence of asRNAs, (2) more than seven nucleotides in seed match, and (3) less than −10 binding score. From among 285 overlapping miRNAs, 25 miRNAs that satisfied the above criteria were selected. By validating the levels of miRNAs and performing a survival analysis using our sequencing data, two miRNAs—miR-149-5p and miR-485-5p—were identified as decoying miRNAs of AFAP1-AS1 and MLK7-AS1 (Figures 2A and S6). Patients with CRC having low miR-149-5p or miR-485-5p expression levels showed poor prognosis (Figure 2B).

The predicted binding sites of miR-149-5p and miR-485-5p in the AFAP1-AS1 and MLK7-AS1 sequences are illustrated in Figure S7. In the sequencing and validation cohort, AFAP1-AS1 and MLK7-AS1 were highly expressed in CRC tissues than in normal tissues, whereas the expression levels of miR-149-5p and miR-485-5p were lower in the same tumor specimens (Figure 2C). Moreover, except MLK7-AS1 vs. miR-149-5p, Spearman's correlation analysis showed a negative relationship between the expression of two asRNAs and two miRNAs (Figures S8A–S8D).

To determine whether asRNAs directly bind to miRNAs, we assessed their levels in miR-149-5p- and miR-485-5p-loaded miRNA-induced silencing complex (miRISC). AGO2 ribonucleoprotein immunoprecipitation (RIP) revealed that AFAP1-AS1 and MLK7-AS1 were more enriched in AGO2 IP than in IgG (Figure 2D), indicating that the two asRNAs are associated with AGO2-miRNA RISC. To examine whether miR-149-5p and miR-485-5p were involved in the association of asRNAs with miRISC, we performed AGO2 RIP followed by the overexpression of miRNA-145-5p and miRNA-485-5p. When miR-149-5p and miR-485-5p were upregulated by introducing miRNA mimics, AFAP1-AS1 and MLK7-AS1 were more abundant in the AGO2 IP than in the negative control miRNA mimic (mimic-NC) (Figure 2E; overall results of AGO2 RIP are shown in Figure S9). To verify the interaction between asRNAs and miRNAs, antisense oligonucleotide (ASO) pull-down experiments were performed using biotin-labeled RNA targeting each asRNA. Overall, two ASOs for each asRNA efficiently captured the corresponding asRNA, and miR-149-5p and miR-485-5p were more enriched in asRNA ASO pull-down than in LacZ ASO pull-down (Figure 2F for AFAP1-AS1 and 2G for MLK7-AS1).

Direct interactions between asRNAs and miRNAs were validated using a luciferase-based assay. We constructed two luciferase reporter plasmids containing (1) a wild-type (WT) sequence of AFAP1-AS1 and MLK7-AS1 and (2) a mutant (MT) that harbors the inverted sequence of the WT seed sequence to abolish miRNA binding. AFAP1-AS1 has two potential binding sites for miR-149-5p and six binding sites for miR-485-5p (Figure S7A). The luciferase reporter assay showed that overexpression of miR-149-5p or miR-485-5p suppressed luciferase expression in WT. However, luciferase expression was not affected by miRNA overexpression in MT (Figure 2H). A total of two potential binding sites for miR-149-5p and miR-485-5p were located on MLK7-AS1. Similarly, with regard to MLK7-AS1 (miRNA binding sites were shown in Figure S7B), overexpression of miR-149-5p or miR-485-5p inhibited luciferase activity in WT, whereas none of the miRNAs affected the activity in MT (Figure 2I). These results revealed that AFAP1-AS1 and MLK7-AS1 hinder the inhibitory function of miR-149-5p and miR-485-5p by functioning as ceRNAs. Therefore, we investigated the role of miR-149-5p and miR-485-5p in CRC progression and identified their common target genes.

miR-149-5p and miR-485-5p inhibit proliferation and metastasis

To examine the roles of miR-149-5p and miR-485-5p in CRC progression, we transfected DLD1 and HT29 cells with miR-149-5p or miR-485-5p mimics. The WST-1 cell proliferation assay indicated that the overexpression of miR-149-5p or miR-485-5p reduced the proliferation of DLD1 and HT29 cells (Figure S10A). Furthermore, cell proliferation decreased after the overexpression of both miRNAs (Figure 3A). In addition, colony-forming assays showed that overexpression of miR-149-5p and miR-485-5p, individually or together, inhibited the clonogenic ability of DLD1 and HT29 cells (Figures 3B and S10B).

To further examine whether miR-149-5p and miR-485-5p are involved in the metastatic potential of CRC, we examined the effect of miRNA overexpression on the invasive and migratory abilities of DLD1 and HT29 cells by transwell and wound healing assays. Transwell assays indicated that invasiveness was decreased by overexpression of either miR-149-5p or miR-485-5p or both miRNAs

and/or miR-485-5p, the enrichment of AFAP1-AS1 and MLK7-AS1 in AGO2 IP was assessed by qRT-PCR. (F and G) To verify the interaction between asRNAs and miRNAs, ASO pull-down (F) (AFAP1-AS1) and (G) (MLK7-AS1) was conducted. The levels of asRNA and miRNA in ASO pull-down materials were determined by qRT-PCR. (H and I) To verify the direct interaction of miR-149-5p and miR-485-5p with AFAP1-AS1 (H) and MLK7-AS1 (I), reporter vectors were constructed, and luciferase activity was examined. Detailed information on miRNA response elements (MREs) and reporter vectors (wild-type [WT] and mutant [MT] sequence) is shown in Figure S4.
Data are expressed as mean ± standard deviation. Statistical significance was set at $p < 0.05$ (*$p < 0.05$, **$p < 0.01$, ***$p < 0.001$, or ****$p < 0.0001$).

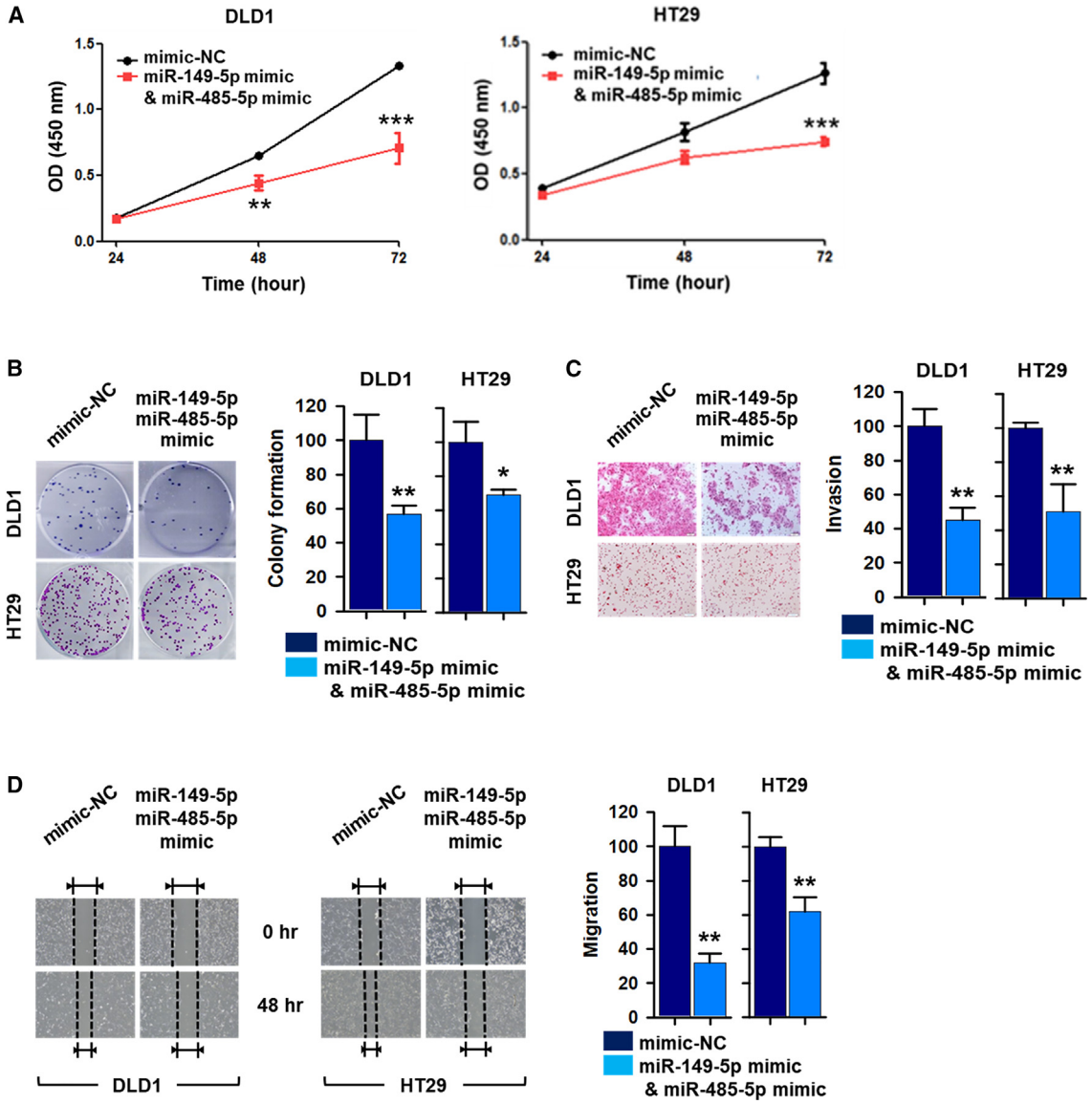

Figure 3. miR-149-5p and miR-485-5p lowered cell proliferation and inhibited the metastatic potential of DLD1 and HT29 cells

DLD1 and HT29 cells were transfected simultaneously with miR-149-5p and miR-485-5p mimics, and cell proliferation and metastatic potential were assessed. (A and B) Cell proliferation was examined by WST-1 (A) and colony-forming assay (B). (C and D) Metastatic potential including invasive and migratory abilities were determined by transwell (C) and wound healing assays (D).

Data are expressed as mean ± standard deviation. Statistical significance was set at $p < 0.05$ (*$p < 0.05$, **$p < 0.01$, ***$p < 0.001$, or ****$p < 0.0001$).

(Figures 3C and S10C). In addition, the wound healing assay showed that overexpression of either or both miRNA inhibited cell mobility compared with that of the mimic-NC (Figures 3D and S10D).

Thus, the inhibition of cell growth and metastatic potential by overexpression of miRNA produced the same effects observed in asRNA-silenced cells, demonstrating that AFAP1-AS1 and MLK7-AS1 enhanced the metastatic potential of CRC cells by sponging the tumor-suppressing miRNAs miR-149-5p and miR-485-5p.

miR-149-5p and miR-485-5p suppress SHMT2 and IGFBP5

The common target genes for miRNA-149-5p and miRNA-485-5p were predicted using TargetScan 7.1. Among the computationally predicted 30 merged targets, 17 mRNAs were selected by comparing the lists of predicted common targets and upregulated miRNAs (fold change >2.0, $p < 0.05$) obtained from the small RNA sequencing data. To select more reliable target genes, the following three criteria were applied: (1) downregulated by miR-149-5p and miR-485-5p mimics, (2) downregulated by knockdown of AFAP1-AS1 and MLK7-AS1,

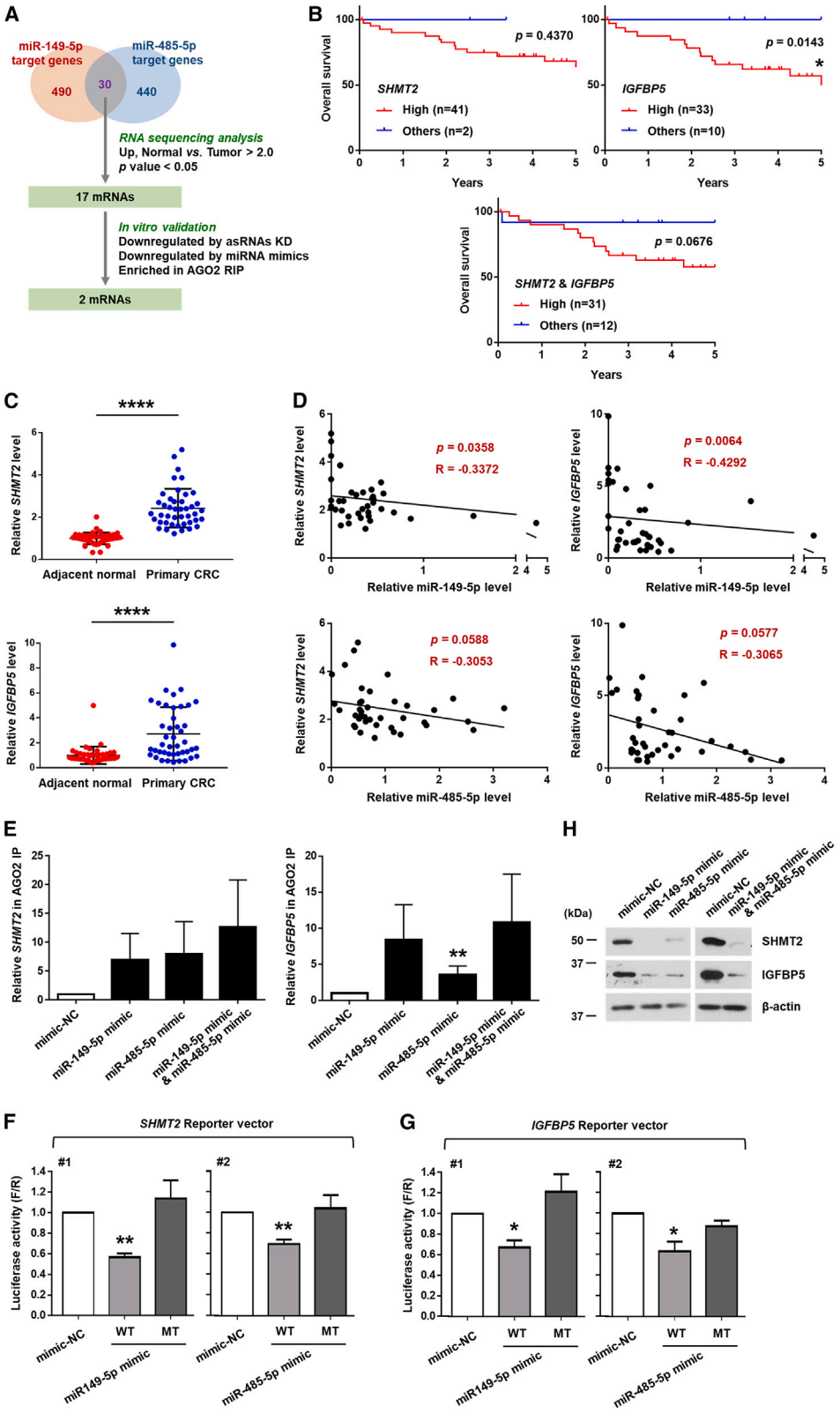

(legend on next page)

and (3) enriched in AGO2 RIP. Finally, two target mRNAs, *SHMT2* and *IGFBP5*, were selected for further analysis (Figures 4A and S11). Survival analysis of *SHMT2* and *IGFBP5* indicated that the high-level group showed poor prognosis compared with the low-level group (Figure 4B). Although the levels of miR-149-5p and miR-485-5p were lower in CRC tissues, *SHMT2* and *IGFBP5* mRNAs were highly expressed (Figure 4C). Accordingly, a negative relationship was observed between the two miRNAs and two target genes based on Spearman's correlation analysis (Figure 4D).

To test whether miR-149-5p and miR-485-5p directly bind to target mRNAs, AGO2 RIP experiments were conducted after overexpression of miR-149-5p and miR-485-5p, individually and together. *SHMT2* mRNA and *IGFBP5* mRNA were enriched in AGO2 IP upon overexpression of both miRNAs (Figure 4E; overall results of AGO2 RIP are shown in Figure S12). To determine whether miR-149-5p and miR-485-5p suppress *SHMT2* and *IGFBP5* by directly binding to the 3′ UTR of their mRNAs, we constructed luciferase reporter vectors containing WT and MT sequences of both miRNA MRE (Figure S13). Each reporter was transduced into DLD1 cells with mimic-NC, miR-149-5p, or miRNA-485-5p mimics, and luciferase activity was determined. A luciferase assay using the *SHMT2* reporter vector revealed that overexpression of miR-149-5p or miR-485-5p suppressed luciferase expression in the WT vector. However, MT luciferase expression was not affected (Figure 4F). Similarly, in the case of the *IGFBP5* reporter, miR-149-5p and miR-485-5p inhibited luciferase activity in WT, but not in MT (Figure 4G). In addition, western blotting results showed that the expression levels of SHMT2 and IGFBP5 decreased after overexpression of either miR-149-5p or miR-485-5p and both (Figure 4H). These results indicate that miR-149-5p and miR-485-5p suppressed *SHMT2* and *IGFBP5* by directly binding to the 3′ UTR of their mRNAs.

We also examined the oncogenic function of *SHMT2* and *IGFBP5* by performing WST-1, colony-forming, and transwell assays. Knockdown of *SHMT2* and *IGFBP5* using two individual siRNAs inhibited cell proliferation, colony formation, and invasion (Figure S14), indicating that *SHMT2* and *IGFBP5* are involved in the tumor-suppressive effects of miR-149-5p and miR-485-5p. We also examined the effects of AFAP1-AS1/MLK7-AS1, miR-149-5p/miR-485-5p, and *SHMT2*/*IGFBP5* regulatory axes on cellular signaling in DLD1 cells (Figure S15). Phospho-kinase proteome array revealed that downregulation of AFAP1-AS1 and MLK7-AS1, upregulation of miR-149-5p and miR-485-5p, and downregulation of SHMT2 and IGFBP5 resulted in decreased levels of phosphorylated AKT and ERK (Figure S16).

miR-149-5p and miR-485-5p are required for the suppression of SHMT2 and IGFBP5 by the knockdown of AFAP1-AS1 and MLK7-AS1

To verify whether AFAP1-AS1 and MLK7-AS1 regulate the expression of SHMT2 and IGFBP5 by sponging miR-149-5p and miR-485-5p, we conducted rescue experiments using miRNA inhibitors. Knockdown of both AFAP1-AS1 and MLK7-AS1 increased the expression levels of both miR-149-5p and miR-485-5p and, thus, decreased the expression levels of *SHMT2* and *IGFBP5* in DLD1 and HT29 cells. However, when the levels of miR-149-5p and miR-485-5p were decreased by the miRNA inhibitors, the suppression of *SHMT2* and *IGFBP5* was reversed (Figure 5A). We also conducted AGO2 RIP following the knockdown of AFAP1-AS1 and MLK7-AS1. *SHMT2* and *IGFBP5* mRNAs were enriched in AGO2 IP materials upon knockdown of AFAP1-AS1- and MLK7-AS1 (Figures 5B and 5C; overall results of AGO2 RIP are shown in Figure S17). This was a result of the increase in the levels of miR-149-5p and miR-485-5p. Western blotting results also showed that the expression of *SHMT2* and *IGFBP5* decreased after knockdown of either AFAP1-AS1 or MLK7-AS1 and both (Figure 5D).

AFAP1-AS1 and MLK7-AS1 regulate cell growth and metastasis by sponging miR-149-5p and miR-485-5p *in vivo*

Based on these results, we confirmed that AFAP1-AS1 and MLK7-AS1 are closely associated with CRC progression *in vitro*. To investigate whether AFAP1-AS1 and MLK7-AS1 were related to CRC progression *in vivo*, we developed mouse models through the subcutaneous and splenic injection of DLD1 cells. We found that both AFAP1-AS1 and MLK7-AS1 were downregulated by the introduction of both siRNAs. The subcutaneous mouse model presented lower tumor volume and significantly decreased weight in the AFAP1-AS1/MLK7-AS1-silenced group compared with those in the negative control group (Figures 6A and 6B, respectively). AFAP1-AS1 and MLK7-AS1 were verified to be downregulated, and the expression levels of miR-149-5p and miR-485-5p were increased (Figures 6C–6F). In the splenic injection mouse model, fewer metastases were observed in the AFAP1-AS1/MLK7-AS1-silenced group (28.6%, two out of seven mice) than in the negative control group (85.7%, six out of seven mice) (Figure 6G). The degree of liver metastasis was determined by visual counting and magnetic resonance imaging (MRI).

Figure 4. SHMT2 and IGFBP5 were common targets of the AFAP1-AS1/MLK7-AS1-miR-149-5p/miR-485-5p regulatory axis

(A) Venn diagram and schematic workflow for selecting *SHMT2* and *IGFBP5* as common target genes. (B) Kaplan-Meier overall survival curves of patients with CRC with low and high level of *SHMT2* and/or *IGFBP5*. More than 2-fold high expression was classified as "High," and all others were classified as "Others" to analyze the prognosis. (C) RNA sequencing data representing higher expression of *SHMT2* and *IGFBP5* in CRC compared with that in adjacent normal tissues. (D) The correlation between the expression levels of miRNAs (miR-149-5p and miR-485-5p) and target genes (*SHMT2* and/or *IGFBP5*) was examined by analyzing RNA sequencing data. (E) The enrichment of *SHMT2* and *IGFBP5* mRNA in AGO2 IP was examined using PEB cell lysates of DLD1 cells transfected with miR-149-5p and/or miR-485-5p mimics. (F and G) To verify the direct interaction of miR-149-5p and miR-485-5p with the 3′ UTR of *SHMT2* (F) and *IGFBP5* (G) mRNA, reporter vectors were constructed, and luciferase activity was examined. Detailed information on MREs and reporter vectors (WT and MT) is shown in Figure S7. (H) After DLD1 cells were transfected with either miR-149-5p or miR-485-5p mimics and both, the protein expression levels of SHMT2 and IGFBP5 were assessed by western blotting analysis.

Data are expressed as mean ± standard deviation. Statistical significance was set at $p < 0.05$ (*$p < 0.05$, **$p < 0.01$, ***$p < 0.001$, or ****$p < 0.0001$).

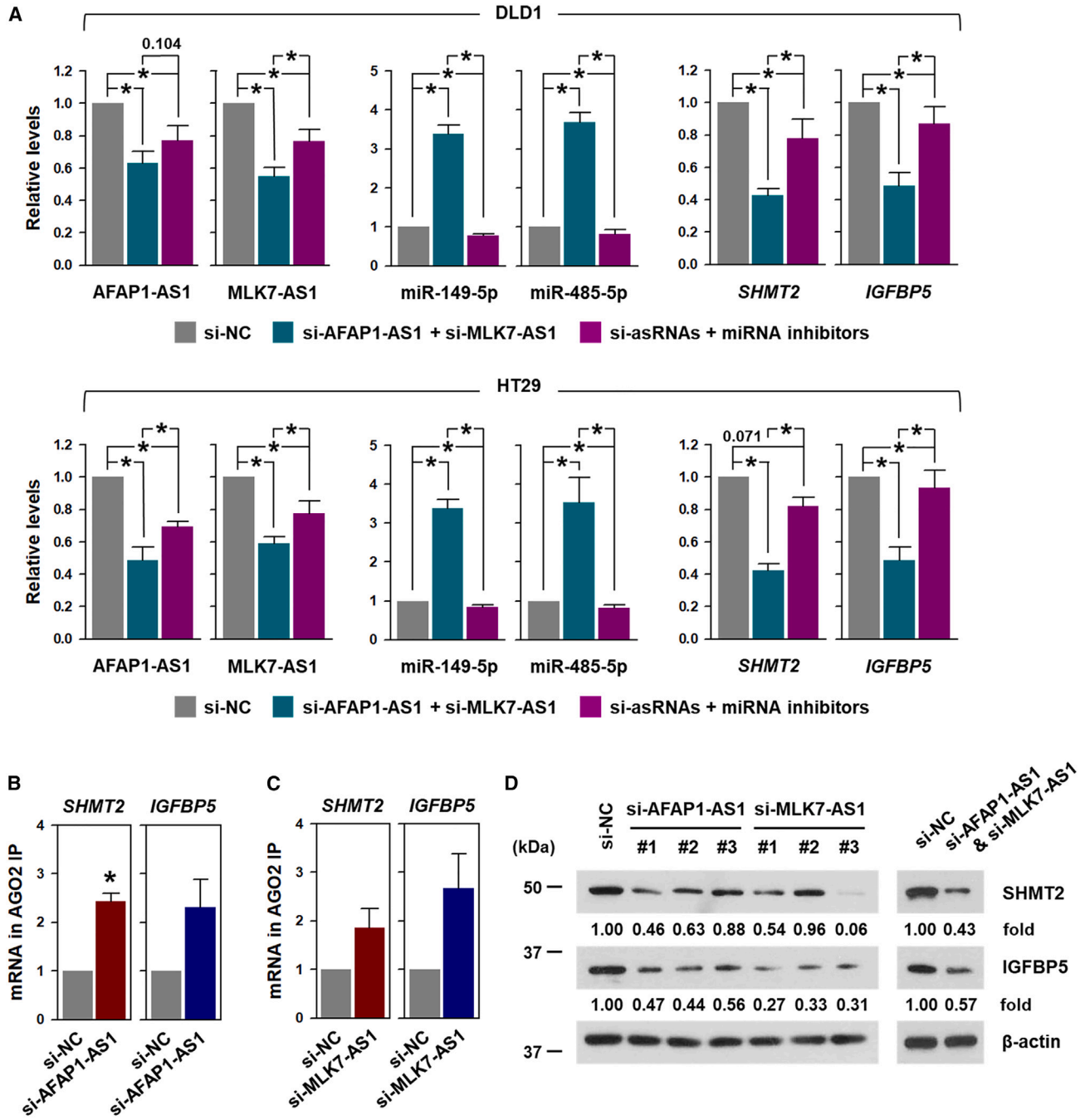

Figure 5. miR-149-5p and miR-485-5p were required for the downregulation of SHMT2 and IGFBP5 by knockdown of AFAP1-AS1 and MLK7-AS1

(A) DLD1 and HT29 cells were transfected with indicated siRNA or miRNA and the levels of asRNA (AFAP1-AS1 and MLK7-AS1), miRNAs (miR-149-5p and miR-485-5p), and common targets (*SHMT2* and *IGFBP5*), were assessed by qRT-PCR. (B and C) DLD1 cells were transfected with siRNA targeting AFAP1-AS1 (B) or MLK7-AS1 (C), and the enrichment of *SHMT2* and *IGFBP5* mRNA was examined using AGO2 IP. (D) The protein expression of SHMT2 and IGFBP5 in AFAP1-AS1- and MLK7-AS1-silenced DLD1 cells was determined by Western blot analysis. β-Actin was used as a loading control.

Data are expressed as mean ± standard deviation. Statistical significance was set at $p < 0.05$ (*$p < 0.05$, **$p < 0.01$, ***$p < 0.001$, or ****$p < 0.0001$).

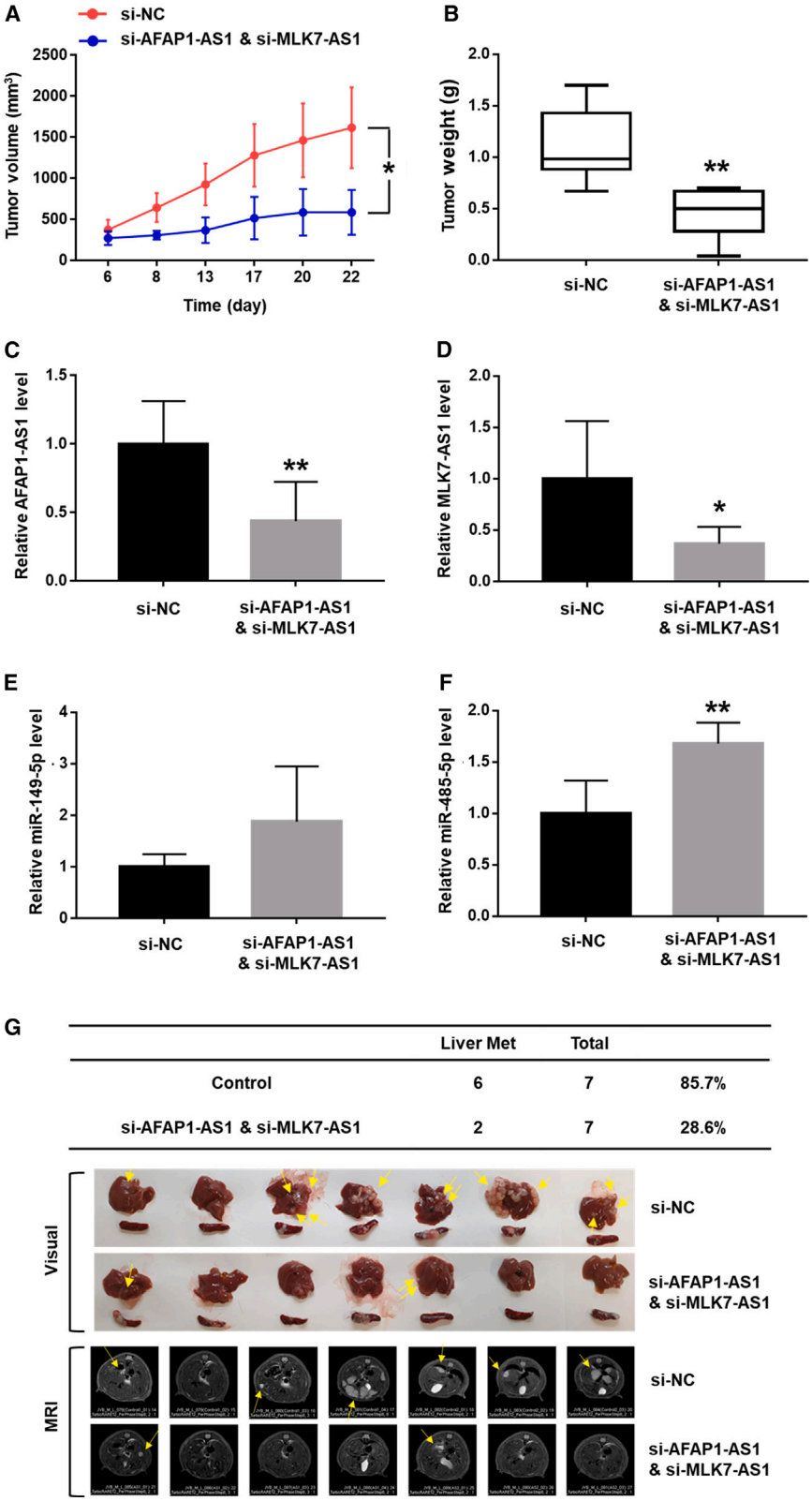

Figure 6. Knockdown of AFAP1-AS1 and MLK7-AS1 inhibited tumor formation and liver metastasis of CRC *in vivo*

(A–F) DLD1 cells were transfected with siRNA mixture targeting AFAP1-AS1 and MLK7-AS1. The cells were subcutaneously injected into the flanks of mice. Tumor volume was calculated as described in materials and methods (A). Tumor weight was measured after the mice were sacrificed (B). The levels of AFAP1-AS1 (C), MLK7-AS1 (D), miR-149-5p (E), and miR-485-5p (F) in the enucleated tumor were assessed by qRT-PCR. (G) Degree of liver metastasis was determined by visually counting the number of nodules and MRI.

Data are expressed as mean ± standard deviation. Statistical significance was set at $p < 0.05$ (*$p < 0.05$, **$p < 0.01$, ***$p < 0.001$, or ****$p < 0.0001$).

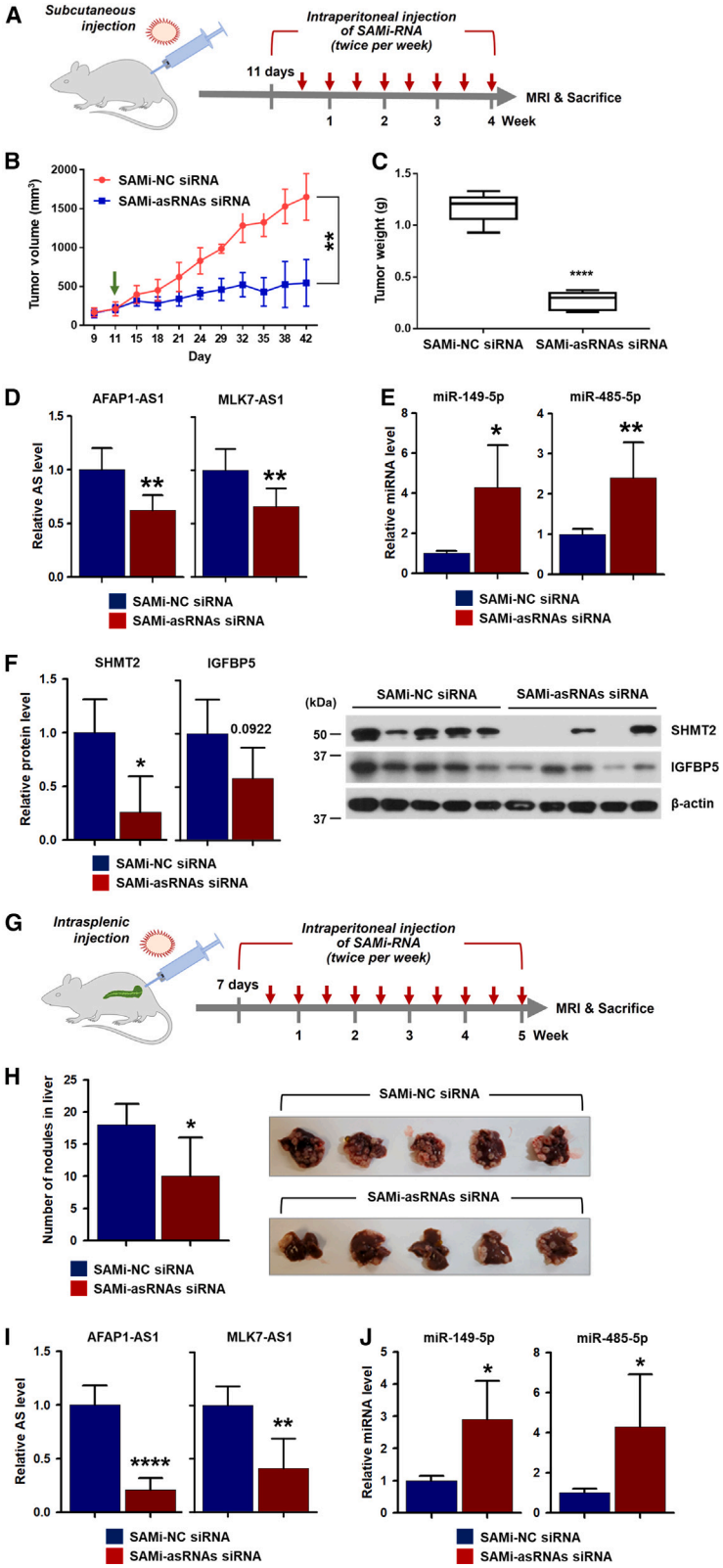

Figure 7. Nanoparticles loaded with siRNA mixture targeting AFAP1-AS1 and MLK7-AS1 exhibited inhibitory effects on tumor formation and liver metastasis *in vivo*

(A) Injection schedule of nanoparticles in the subcutaneous xenograft CRC model. (B) Tumor volume was calculated as described in materials and methods at intervals of 3 days for 4 weeks after injection of nanoparticles. (C) Tumor weight was measured after the mice were sacrificed. (D and E) The levels of asRNA (D) (AFAP1-AS1 and MLK7-AS1) and miRNAs (E) (miR-149-5p and miR-485-5p) in the enucleated tumor were examined by qRT-PCR. (F) The mRNA and protein levels of SHMT2 and IGFBP5 were determined by qRT-PCR and western blotting analyses, respectively. (G) Injection schedule of nanoparticles in the intrasplenic liver metastasis CRC model. (H) The degree of liver metastasis was assessed by counting the number of nodules. (I and J) The levels of asRNA (I) (AFAP1-AS1 and MLK7-AS1) and miRNAs (J) (miR-149-5p and miR-485-5p) in the enucleated tumor were examined by qRT-PCR. Data are expressed as mean ± standard deviation. Statistical significance was set at $p < 0.05$ (*$p < 0.05$, **$p < 0.01$, ***$p < 0.001$, or ****$p < 0.0001$).

These results indicate that knockdown of AFAP1-AS1 and MLK7-AS1 inhibits tumor formation and liver metastasis of CRC.

Therapeutic application of AFAP1-AS1 and MLK7-AS1 siRNA using nanoparticles

We used siRNA-loaded nanoparticles as a delivery system to apply our *in vitro* findings to the bedside. For this experiment, DLD1 cells were injected subcutaneously (n = 5 per group) or into the spleen (n = 5 per group) to examine tumor formation and liver metastasis, respectively. After a period of 11 days post subcutaneous injection, siRNA-loaded nanoparticles were introduced twice a week for 4 weeks (Figure 7A). The body weights of mice administered asRNAs and siRNA-loaded nanoparticles (SAMi-asRNAs siRNA) were the same as those of mice in the negative control group (SAMi-NC siRNA) (Figure S18). Regarding tumor growth parameters, we observed a significant decrease in tumor volume (Figure 7B) and tumor weight at the end of the experiment (Figure 7C). Decreased levels of AFAP1-AS1 and MLK7-AS1 in enucleated tumors were verified by qRT-PCR (Figure 7D). The expression levels of miR-149-5p and miR-485-5p were also assessed. As expected, both miRNAs were highly expressed in the enucleated tumors of the asRNA siRNA group (Figure 7E). qRT-PCR and western blotting analyses showed that *SHMT2* and *IGFBP5* were effectively downregulated in the siRNA group (Figure 7F).

Liver metastasis was induced via intrasplenic injection, following which we administered asRNA siRNA-loaded nanoparticles twice a week for approximately 5 weeks (Figure 7G). We observed that the siRNA group showed a decreased number of metastatic nodules compared with the control group (Figure 7H). The levels of AFAP1-AS1, MLK7-AS1, miR-148-5p, and miR-485-5p in the enucleated tumors were examined by qRT-PCR (Figures 7I and 7J). Both asRNAs were efficiently downregulated, whereas the levels of both miRNAs were upregulated. Taken together, the administration of siRNA-loaded asRNA nanoparticles reduced tumor growth and abolished liver metastasis of CRC.

Our findings suggest a novel regulatory mechanism through which asRNAs control CRC progression by functioning as ceRNAs. In brief, we identified two oncogenic asRNAs—AFAP1-AS1 and MLK7-AS1—that were significantly upregulated in primary CRC tissues than in the adjacent normal tissues. Both AFAP1-AS1 and MLK7-AS1 directly bind to miRNA-149-5p and miRNA-485-5p to mitigate their inhibitory effects on the expression of common targets. Collectively, AFAP1-AS1 and MLK7-AS1 promoted the malignant processes of CRC by upregulating *SHMT2* and *IGFBP5*. *In vitro* and *in vivo* experiments revealed that the decrease in AFAP1-AS1 and MLK7-AS1 expression showed tumor-suppressing and anti-metastatic effects. Moreover, the administration of nanoparticles loaded with asRNA-targeting siRNAs reduced tumor formation and inhibited liver metastasis of CRC. Based on our results, we demonstrate that AFAP1-AS1 and MLK7-AS1 have the potential to evolve as promising treatments for CRC patients.

DISCUSSION

AsRNAs have attracted the attention of many scientists as biomarkers for the diagnosis and treatment of cancer.[14,15] Many asRNAs have been identified to be closely associated with CRC progression.[16] However, asRNAs showing clinical applicability have not been discovered yet. The purpose of this study was to identify oncogenic asRNAs, define their mechanism of action, and to use them to develop a promising treatment for CRC patients. By analyzing the RNA sequencing data, nine asRNAs were found to be highly expressed in CRC tissues. Among them, the expression levels of AFAP1-AS1 and MLK7-AS1 showed correlation with the overall survival (OS) rate of patients with CRC. Importantly, patients with high levels of both AFAP1-AS1 and MLK7-AS1 (approximately 51% of all patients) showed significantly lower survival rates than those with low levels of these asRNAs, implying that the expression levels of both these asRNAs are significantly associated with the prognosis of CRC patients. Hence, we decided to further study the mechanism underlying the action of the two asRNAs when acting simultaneously rather than individually.

AFAP1-AS1 and MLK7-AS1 have been reported to regulate the proliferation and metastatic potential of various cancers by functioning as oncogenes as well as ceRNAs. AFAP1-AS1 is aberrantly overexpressed and closely associated with poor prognosis in patients with CRC.[17] Knockdown of AFAP1-AS1 inhibited cell proliferation, colony formation, migration, and invasion. A decrease in AFAP1-AS1 expression increases E-cadherin expression and decreases vimentin expression.[17] By functioning as a ceRNA, AFAP1-AS1 influences miRNA-mRNA interaction, such as miR-195-5p/WISP1,[18] miR-2110/Sp1,[19] miR-27b-3p/VEGFC,[20] miR-653/RAI14,[21] and smiR-107/PDK4.[22] Similarly, the knockdown of MLK7-AS1, which is upregulated in CRC, reduces CRC cell proliferation through the downregulation of p21.[23] MLK7-AS1 functions as a ceRNA of miR-375 and mitigates the inhibitory effects of miR-375 on YWHAZ[24] and YAP1.[25,26] In addition to AFAP1-AS1 and MLK7-AS1, several other asRNAs are known to regulate CRC progression by sponging miRNAs. For example, DSCAM-AS1/miR-204/SOX4,[27] FLVCR1-AS1/miR-381/RAP2A,[28] ZEB1-AS1/miR-205/YAP1,[29] ZFPM2-AS1/miR-137/TRIM24,[30] and ZNF561-AS1/miR-26a-3p/miR-128-5p[31] are a few regulatory axes that are closely involved in proliferation and metastatic potential of CRC. SP100-AS1 stabilizes ATG3 and confers radioresistance to CRC cells by absorbing miR-622.[32] In this study, miR-149-5p and miR-485-5p, which are reported to be tumor-suppressing miRNAs in CRC,[33–35] were identified as sponging miRNAs of AFAP1-AS1 and MLK7-AS1. The lncRNAs PCAT-1 and DLGAP1-AS1 function as ceRNAs of miR-149-5p and contribute to CRC progression.[36,37] Along with lncRNAs, circRNAs, circ5615,[38] and circCTNNA1,[39] have also been found to regulate the inhibitory function of miR-149-5p. LINC01224 hinders miR-485-5p-mediated suppression of MCL1 and MYO6.[40,41]

SHMT2 promotes tumorigenesis and metastasis[42] and is closely associated with cancer progression[43] and stemness.[44] In CRC, cytoplasmic SHMT2 blocks β-catenin degradation, which promotes progression

and metastasis.[45] Furthermore, SHMT2 induces chemoresistance to 5-fluorouracil by stimulating nucleotide biosynthesis.[46] In a wide range of cancers, IGFBP5 influences cell proliferation and metastasis via cell-type- and tissue-type-specific routes.[47] Moreover, it is a promising biomarker for predicting responsiveness to therapy and the clinical outcomes of cancer patients. We discovered that *SHMT2* and *IGFBP5* are novel common targets of miR-149-5p and miR-485-5p and are required for the oncogenic functions of AFAP1-AS1 and MLK7-AS1. Cellular signaling (AKT and ERK) and EMT process were affected by the levels of AFAP1-AS1/MLK7-AS1, miR-149-5p/miR-485-5p, and *SHMT2* and *IGFBP5*.

Recent evidence has shown that ncRNAs have the potential to emerge as treatments for CRC. However, the intricate regulatory mechanism of ncRNA-involved gene regulation complicates the development of ncRNA-based cancer treatments. One of the barriers to the clinical application of ncRNAs, including miRNAs, is their delivery. To overcome this hurdle, many studies have explored the use of nanoparticles as carriers for cancer treatment.[48–50] For example, the *in vivo* administration of nanoparticles loaded with FLANC-targeting siRNA significantly inhibited metastasis without toxicity and inflammation.[51] In this study, we identified the mechanism underlying the action of asRNAs and verified that the efficacy of CRC treatment increased effectively by using two asRNAs rather than one as a treatment strategy. Our findings revealed that AFAP1-AS1 and MLK7-AS1 are highly expressed and are closely associated with poor prognosis in CRC patients. Mechanistically, AFAP1-AS1 and MLK7-AS1 upregulated *SHMT3* and *IGFBP5* by sponging the tumor-suppressing miRNAs miR-149-5p and miR-485-5p. *In vivo* experiments indicated that the knockdown of AFAP1-AS1 and MLK7-AS1 inhibited tumor formation and liver metastasis in a xenograft mouse model. Furthermore, the decrease in AFAP1-AS1 and MLK7-AS1 by administration of the nanoparticle-loaded siRNAs diminished tumor formation and liver metastasis in the subcutaneous and intrasplenic mouse models. Collectively, we demonstrated that AFAP1-AS1 and MLK7-AS1 have potential for clinical use as promising candidates for CRC treatment.

MATERIALS AND METHODS

Sample collection

This study was approved by the institutional review board (IRB) of Samsung Medical Center (IRB approval no. SMC 2013-11-007-001). Written informed consent was obtained from all the patients. The study included 43 patients diagnosed with CRC at the Samsung Medical Center (Seoul, Republic of Korea). Tumors and matched adjacent normal tissues were obtained from surgical specimens.

RNA sequencing and survival analysis

Reads from the FASTQ files were mapped to the human reference genome using STAR aligner version 2.5.0a and read counts for each gene were normalized as transcripts per million using the RSEM program. Differentially expressed genes were identified using the DESeq R package with a cutoff ($|\log2 \text{ fold change}| > 2$ and $p < 0.05$). OS was calculated using the Kaplan-Meier method. In the OS analyses of asRNA and target genes, more than 2-fold high expression was defined as "High," and all others were indicated as "Others.". In case of miRNA, less than 0.5-fold low expression was classified as "Low," and all others were represented as "Others."

Cell culture and transfection

CRC cell lines (HT29 and DLD1) were purchased from the American Type Culture Collection and cultured in RPMI 1640 (Gibco, Grand Island, NY) supplemented with 10% fetal bovine serum (FBS) (Gibco) and 1% penicillin-streptomycin (Gibco) at 37°C in an incubator with 5% CO_2. All CRC cells were recently authenticated through short tandem repeat profiling and were regularly tested for mycoplasma contamination.

A transient transfection of HT29 and DLD1 cells with siRNA or miRNA was performed using Lipofectamine RNAiMAX (Invitrogen), according to the manufacturer's instructions. Knockdown of asRNA was performed using three siRNAs that were specifically designed for each asRNA (Table S1). All siRNAs sufficiently decreased the expression of asRNA, and si-AFAP1-AS1 (no. 2) and si-MLK7-AS1 (no. 2) were used to simultaneously silence both asRNAs. To increase or decrease miRNA levels, miRNA mimics or inhibitors, respectively, were used: miR-149-5p mimic (4464066, MC12788, Applied Biosystems, Waltham, MA), miR-485-5p mimic (4464066, MC10837, Applied Biosystems), miR-149-5p inhibitor (4464084, MH12788, Applied Biosystems), and miR-485-5p (4464084, MH10837, Applied Biosystems). The effects of the target genes *SHMT2* and *IGFBP5* on malignant phenotypes were confirmed using two siRNAs, one for each gene. The sequences of the siRNAs used in this study are shown in Table S1.

Western blotting analysis

To prepare whole-cell extracts, the cells were lysed using Pro-Prep buffer (Intron Biotechnology, Seoul, South Korea) containing phosphatase and protease inhibitors. Equal amounts of lysate were separated using sodium dodecyl sulfate-polyacrylamide gel electrophoresis and transferred to polyvinylidene fluoride membranes. After blocking with 5% skim milk, the membranes were incubated with the indicated primary antibodies, washed, and incubated with the appropriate secondary antibodies. The following antibodies were used: SHMT2 (Cell Signaling Technology, Danvers, MA, no. 12762), IGFBP5 (Santa Cruz Biotechnology, sc-515116), vimentin (Thermo Fisher Scientific, Waltham, MA, no. MA5-11883), E-cadherin (24E10) (Cell Signaling Technology, no. 3195), and β-actin (Cell Signaling Technology, no. 3700). β-Actin was used as the loading control for western blotting. Protein bands were detected using an enhanced chemiluminescence reagent.

Reverse transcriptase quantitative polymerase chain reaction (RT-qPCR)

Total RNA was isolated using TRIzol reagent (Invitrogen), according to the manufacturer's instructions. Total RNA was used to synthesize cDNA using AccuPower CycleScript RT premix dT20 (Bioneer, Daejeon, South Korea, no. K-2044-B) according to the manufacturer's

instructions. The mRNA levels were quantified by real-time quantitative polymerase chain reaction (qPCR) (ABI Prism 7900) using the Power SYBR Green PCR Master Mix (Applied Biosystems). Primer sequences used in this study are shown in Table S2. miRNA-specific TaqMan primer (Applied Biosystems, no. 4427975) was used for real-time qPCR.

Cell proliferation assay

CRC cells were seeded onto 96-well plates at a density of 3–5 $\times$ 10^3 cells/well. Cell proliferation was measured using a WST-1 assay (Roche, Basel, Switzerland). CRC cell viability was assessed at various time points, and assays were performed by adding WST-1 directly to the culture wells and incubating for 60 min at 37°C with 5% CO_2. Absorbance was measured at a wavelength of 450 nm. The experiments were repeated more than three times under each experimental condition.

A colony-forming assay was performed to determine clonogenicity. In brief, equal numbers of transfected cells were seeded in triplicate onto six-well plates and cultured for 2 weeks. The cells were fixed with 4% paraformaldehyde and stained with 0.2% crystal violet. The clonogenic ability was determined by counting the number of colonies.

Determination of metastatic potential

The migratory ability was measured using a wound healing assay. CRC cells were seeded onto six-well plates. When cell confluence reached approximately 85%, scratch wounds were made by scraping the cell layer on each culture plate using a tip. After wounding, the debris was removed by washing the cells with serum-free medium. Wounded cultures were incubated in serum-free medium for 48 h, and their migratory ability was determined by measuring the migration distance. The experiments were performed in triplicate.

Cell invasion assays were performed using a Matrigel invasion chamber (Corning, Corning, NY). After hydration of the Matrigel, equal numbers of transfected cells (5–8 $\times$ 10^4 cells) in serum-free medium were added to the upper chamber. Invasion was triggered by the addition of the same medium containing 10% FBS as a chemoattractant to the bottom chambers. After incubation for 24 or 48 h, the invading cells were fixed with 95% MeOH for 5 min and stained with 0.1% hematoxylin and eosin. Invasiveness was determined by counting the number of invading cells in at least ten randomly selected fields.

AGO2 RIP

For RIP, Dynabeads Protein G (Thermo Fisher Scientific) were coated with control IgG (Santa Cruz Biotechnology) or AGO2 antibodies (Sigma-Aldrich, St. Louis, MO). Cytoplasmic lysates were prepared using a protein extraction buffer (PEB) containing protease/phosphatase inhibitors and RNaseOUT inhibitor (Invitrogen). Equal amounts of lysates were incubated with antibody-coated Dynabeads at 4°C for 4 h. After washing several times with PEB buffer, the AGO2-IP materials were treated with DNase I (Ambion, Austin, TX) and Protease K (Bioneer). Proteins were denatured with acid phenol (Ambion), and RNA was precipitated with absolute ethanol overnight at −20°C. The target mRNA level in the miRISC was determined by qRT-PCR.

ASO pull-down assay

To identify asRNA-associated miRNAs, an ASO pull-down assay was performed using non-overlapping biotinylated ASOs that recognize LacZ and asRNAs. Incubation of whole-cell lysates with biotinylated ASO was followed by coupling with streptavidin-coupled Dynabeads (Invitrogen). RNA was isolated from the pull-down materials, and miRNA levels were determined by qRT-PCR.

Luciferase assay

To check whether the miRNA directly recognizes the 3′ UTR of the target mRNA, pmirGLO dual-luciferase vectors (E133A, Promega, Madison, WI) containing WT or MT MRE sequences were constructed. After 24 h post-transfection, luciferase activity was measured using the Dual-Glo luciferase activity assay system (Promega) according to the manufacturer's instructions.

Subcutaneous injection mouse model

Approximately 1 $\times$ 10^6 DLD1 cells were mixed with 50 μL of Hanks' balanced salt solution (HBSS) and 50 μL of Matrigel and subcutaneously injected into the flanks of 6- to 7-week-old female BALB/c nude mice (Orient Bio Group, Seoul, Republic of Korea). Tumor size was measured using a caliper, and tumor volume was calculated using the following formula: (short length $\times$ long length $\times$ width)/2. The mice were euthanized 6–8 weeks after inoculation or as soon as a reduction in vitality was observed.

Intrasplenic injection mouse model

In this model, 6- to 7-week-old female BALB/c nude mice (Orient Bio) were anesthetized with a mixture of catamin (30 mg/kg; Yuhan, Seoul, Republic of Korea, no. 7001) and Rompun (10 mg/kg; Bayer, Leverkusen, Germany) via intraperitoneal injection (0.01 mL/mg). A small left abdominal flank incision was made, and the spleen was exteriorized for intrasplenic injection. Approximately 1 $\times$ 10^6 DLD1 cells were suspended in 50 μL HBSS (Gibco) and injected into the mouse spleen with a 30-gauge needle. A cotton swab was applied to the injection site for 1 min to prevent tumor cell leakage and bleeding. The injected spleen was returned to the abdomen, and the wound was sutured with 6-0 black silk. The mice were euthanized by placing them in a chamber with 100% CO_2. The mice were monitored for faded eye color and lack of respiration, and CO_2 flow was maintained for a minimum of 1 min after respiration ceased. An intrasplenic injection was administered to female BALB/c nude mice that were 6–7 weeks old. After 6 weeks, MRI was performed, and the mice were sacrificed to obtain tissues. All animal experiments were conducted at a specific pathogen-free animal experiment center at the Samsung Medical Center. The Samsung Medical Center on Laboratory Animals Committee approved the experiments (approval no. 20210319001).

Injection of nanoparticle

All mice were aged 6 weeks at the time of cell injection. The asRNA siRNA dose was 3 mpk for all therapeutic experiments with

nanoparticles. Nanoparticles were used as delivery systems for the asRNA-targeting siRNAs (#SAMi-RNA; Bioneer). Eleven days after subcutaneous injection of the mouse model, asRNA siRNA-loaded nanoparticles were administered intraperitoneally twice a week for approximately 4 weeks. Seven days post-intrasplenic injection, a liver metastatic mouse model was generated by the intraperitoneal administration of asRNA siRNA-loaded nanoparticles twice a week for approximately 5 weeks.

Statistical analysis

Statistical comparisons were performed using GraphPad Prism software. Data are expressed as mean ± standard deviation. Statistical significance was set at $p < 0.05$ (*$p < 0.05$, **$p < 0.01$, ***$p < 0.001$, or ****$p < 0.0001$).

DATA AND CODE AVAILABILITY

The data supporting the findings of this study are available within the article and from the corresponding author upon request.

SUPPLEMENTAL INFORMATION

Supplemental information can be found online at https://doi.org/10.1016/j.omtn.2023.07.004.

ACKNOWLEDGMENTS

This research was supported by the Korea Health Technology R&D Project through the Korea Health Industry Development Institute (KHIDI) funded by the Ministry of Health & Welfare, Republic of Korea (HR20C0025 to Y.B.C.), the Basic Research Program through the National Research Foundation (NRF) funded by the Ministry of Science and ICT, Republic of Korea (NRF-2022R1F1A1074655 to H.H.K.), and the Global Ph.D. Fellowship Program through the National Research Foundation (NRF) funded by the Ministry of Education, Republic of Korea (NRF-2017H1A2A1045221 to T.W.K. and NRF-2018H1A2A1062036 to H.J.). The biospecimens used in this study were provided by Samsung Medical Center BioBank (20140002).

AUTHOR CONTRIBUTIONS

T.W.K., H.J., H.H.K., and Y.B.C. contributed to the concept and design of the study. T.W.K., H.J., N.H.Y., and C.H.S. contributed to the experimental data acquisition. T.W.K., H.J., H.H.K., and Y.B.C. contributed to the analysis and interpretation of results. T.W.K., H.J., H.H.K., and Y.B.C. contributed to the drafting and revision of the manuscript.

DECLARATION OF INTERESTS

The authors declare no competing interests.

REFERENCES

1. Hubbard, J.M., and Grothey, A. (2015). Colorectal cancer in 2014: progress in defining first-line and maintenance therapies. Nat. Rev. Clin. Oncol. *12*, 73–74.
2. Sung, H., Ferlay, J., Siegel, R.L., Laversanne, M., Soerjomataram, I., Jemal, A., and Bray, F. (2021). Global Cancer Statistics 2020: GLOBOCAN Estimates of Incidence and Mortality Worldwide for 36 Cancers in 185 Countries. CA. Cancer J. Clin. *71*, 209–249.
3. Siegel, R., Desantis, C., and Jemal, A. (2014). Colorectal cancer statistics, 2014. CA. Cancer J. Clin. *64*, 104–117.
4. Siegel, R.L., Miller, K.D., and Jemal, A. (2019). Cancer statistics, 2019. CA. Cancer J. Clin. *69*, 7–34.
5. Alexander, R.P., Fang, G., Rozowsky, J., Snyder, M., and Gerstein, M.B. (2010). Annotating non-coding regions of the genome. Nat. Rev. Genet. *11*, 559–571.
6. Djebali, S., Davis, C.A., Merkel, A., Dobin, A., Lassmann, T., Mortazavi, A., Tanzer, A., Lagarde, J., Lin, W., Schlesinger, F., et al. (2012). Landscape of transcription in human cells. Nature *489*, 101–108.
7. Adams, B.D., Parsons, C., Walker, L., Zhang, W.C., and Slack, F.J. (2017). Targeting noncoding RNAs in disease. J. Clin. Invest. *127*, 761–771.
8. Salmena, L., Poliseno, L., Tay, Y., Kats, L., and Pandolfi, P.P. (2011). A ceRNA hypothesis: the Rosetta Stone of a hidden RNA language? Cell *146*, 353–358.
9. Poliseno, L., Salmena, L., Zhang, J., Carver, B., Haveman, W.J., and Pandolfi, P.P. (2010). A coding-independent function of gene and pseudogene mRNAs regulates tumour biology. Nature *465*, 1033–1038.
10. Cheng, Y., Geng, L., Wang, K., Sun, J., Xu, W., Gong, S., and Zhu, Y. (2019). Long Noncoding RNA Expression Signatures of Colon Cancer Based on the ceRNA Network and Their Prognostic Value. Dis. Markers *2019*, 7636757.
11. Yin, H., Hu, J., Ye, Z., Chen, S., and Chen, Y. (2021). Serum long noncoding RNA NNTAS1 protected by exosome is a potential biomarker and functions as an oncogene via the miR496/RAP2C axis in colorectal cancer. Mol. Med. Rep. *24*, 585.
12. Zhao, S.Y., Wang, Z., Wu, X.B., Zhang, S., Chen, Q., Wang, D.D., and Tan, Q.F. (2022). CERS6-AS1 contributes to the malignant phenotypes of colorectal cancer cells by interacting with miR-15b-5p to regulate SPTBN2. Kaohsiung J. Med. Sci. *38*, 403–414.
13. Liang, J., Tian, X.F., and Yang, W. (2020). Effects of long non-coding RNA Opa-interacting protein 5 antisense RNA 1 on colon cancer cell resistance to oxaliplatin and its regulation of microRNA-137. World J. Gastroenterol. *26*, 1474–1489.
14. Pelechano, V., and Steinmetz, L.M. (2013). Gene regulation by antisense transcription. Nat. Rev. Genet. *14*, 880–893.
15. Faghihi, M.A., and Wahlestedt, C. (2009). Regulatory roles of natural antisense transcripts. Nat. Rev. Mol. Cell Biol. *10*, 637–643.
16. Vellichirammal, N.N., Albahrani, A., Banwait, J.K., Mishra, N.K., Li, Y., Roychoudhury, S., Kling, M.J., Mirza, S., Bhakat, K.K., Band, V., et al. (2020). Pan-Cancer Analysis Reveals the Diverse Landscape of Novel Sense and Antisense Fusion Transcripts. Mol. Ther. Nucleic Acids *19*, 1379–1398.
17. Zhang, F., Li, J., Xiao, H., Zou, Y., Liu, Y., and Huang, W. (2018). AFAP1-AS1: A novel oncogenic long non-coding RNA in human cancers. Cell Prolif. *51*, e12397.
18. Li, Y., Zhu, Z., Hou, X., and Sun, Y. (2021). LncRNA AFAP1-AS1 Promotes the Progression of Colorectal Cancer through miR-195-5p and WISP1. JAMA Oncol. *2021*, 6242798.
19. Zhang, X., Li, F., Zhou, Y., Mao, F., Lin, Y., Shen, S., Li, Y., Zhang, S., and Sun, Q. (2021). Long noncoding RNA AFAP1-AS1 promotes tumor progression and invasion by regulating the miR-2110/Sp1 axis in triple-negative breast cancer. Cell Death Dis. *12*, 627.
20. Xia, M., Duan, L.J., Lu, B.N., Pang, Y.Z., and Pang, Z.R. (2021). LncRNA AFAP1-AS1/miR-27b-3p/VEGF-C axis modulates stemness characteristics in cervical cancer cells. Chin. Med. J. *134*, 2091–2101.
21. Liu, F., Hu, L., Pei, Y., Zheng, K., Wang, W., Li, S., Qiu, E., Shang, G., Zhang, J., and Zhang, X. (2020). Long non-coding RNA AFAP1-AS1 accelerates the progression of melanoma by targeting miR-653-5p/RAI14 axis. BMC Cancer *20*, 258.
22. Liu, B., Yan, L., Chi, Y., Sun, Y., and Yang, X. (2021). Long non-coding RNA AFAP1-AS1 facilitates ovarian cancer progression by regulating the miR-107/PDK4 axis. J. Ovarian Res. *14*, 60.
23. Zhang, R., Li, J., Yan, X., Jin, K., Li, W., Liu, X., Zhao, J., Shang, W., and Zhao, X. (2019). Long noncoding RNA MLK7AS1 promotes proliferation in human colorectal cancer via downregulation of p21 expression. Mol. Med. Rep. *19*, 1210–1221.

24. Jia, J., Sun, J., Wang, W., and Yong, H. (2021). Long Noncoding RNA MLK7-AS1 Promotes Non-Small-Cell Lung Cancer Migration and Invasion via the miR-375-3p/YWHAZ Axis. Front. Oncol. *11*, 626036.

25. Yan, H., Li, H., Li, P., Li, X., Lin, J., Zhu, L., Silva, M.A., Wang, X., Wang, P., and Zhang, Z. (2020). Retraction Note: Long noncoding RNA MLK7-AS1 promotes ovarian cancer cells progression by modulating miR-375/YAP1 axis. J. Exp. Clin. Cancer Res. *39*, 233.

26. Yan, H., Li, H., Li, P., Li, X., Lin, J., Zhu, L., Silva, M.A., Wang, X., Wang, P., and Zhang, Z. (2018). Long noncoding RNA MLK7-AS1 promotes ovarian cancer cells progression by modulating miR-375/YAP1 axis. J. Exp. Clin. Cancer Res. *37*, 237.

27. Lu, C., Xie, T., Guo, X., Wu, D., Li, S., Li, X., Lu, Y., and Wang, X. (2020). LncRNA DSCAM-AS1 Promotes Colon Cancer Cells Proliferation and Migration via Regulating the miR-204/SOX4 Axis. Cancer Manag. Res. *12*, 4347–4356.

28. Han, Y., Wang, X., Mao, E., Shen, B., and Huang, L. (2021). lncRNA FLVCR1AS1 drives colorectal cancer progression via modulation of the miR381/RAP2A axis. Mol. Med. Rep. *23*, 139.

29. Jin, Z., and Chen, B. (2020). LncRNA ZEB1-AS1 Regulates Colorectal Cancer Cells by MiR-205/YAP1 Axis. Open Med. *15*, 175–184.

30. Xiao, M., Liang, Z., and Yin, Z. (2021). Long noncoding RNA ZFPM2AS1 promotes colorectal cancer progression by sponging miR137 to regulate TRIM24. Mol. Med. Rep. *23*, 98.

31. Si, Z., Yu, L., Jing, H., Wu, L., and Wang, X. (2021). Oncogenic lncRNA ZNF561-AS1 is essential for colorectal cancer proliferation and survival through regulation of miR-26a-3p/miR-128-5p-SRSF6 axis. J. Exp. Clin. Cancer Res. *40*, 78.

32. Zhou, Y., Shao, Y., Hu, W., Zhang, J., Shi, Y., Kong, X., and Jiang, J. (2023). A novel long noncoding RNA SP100-AS1 induces radioresistance of colorectal cancer via sponging miR-622 and stabilizing ATG3. Cell Death Differ. *30*, 111–124. https://doi.org/10.1038/s41418-022-01049-1.

33. Pan, Y., Sun, H., Hu, X., He, B., Liu, X., Xu, T., Chen, X., Zeng, K., and Wang, S. (2018). The inhibitory role of miR4855p in colorectal cancer proliferation and invasion via targeting of CD147. Oncol. Rep. *39*, 2201–2208.

34. Li, J., Xu, J., Yan, X., Jin, K., Li, W., and Zhang, R. (2018). MicroRNA-485 plays tumour-suppressive roles in colorectal cancer by directly targeting GAB2. Oncol. Rep. *40*, 554–564.

35. Hu, X.X., Xu, X.N., He, B.S., Sun, H.L., Xu, T., Liu, X.X., Chen, X.X., Zeng, K.X., Wang, S.K., and Pan, Y.Q. (2018). microRNA-485-5p Functions as a Tumor Suppressor in Colorectal Cancer Cells by Targeting CD147. J. Cancer *9*, 2603–2611.

36. Wang, A.H., Fan, W.J., Fu, L., and Wang, X.T. (2019). LncRNA PCAT-1 regulated cell proliferation, invasion, migration and apoptosis in colorectal cancer through targeting miR-149-5p. Eur. Rev. Med. Pharmacol. Sci. *23*, 8310–8320.

37. Qu, L., Chen, Y., Zhang, F., and He, L. (2021). The lncRNA DLGAP1-AS1/miR-149-5p/TGFB2 axis contributes to colorectal cancer progression and 5-FU resistance by regulating smad2 pathway. Mol. Ther. Oncolytics *20*, 607–624.

38. Ma, Z., Han, C., Xia, W., Wang, S., Li, X., Fang, P., Yin, R., Xu, L., and Yang, L. (2020). circ5615 functions as a ceRNA to promote colorectal cancer progression by upregulating TNKS. Cell Death Dis. *11*, 356.

39. Chen, P., Yao, Y., Yang, N., Gong, L., Kong, Y., and Wu, A. (2020). Circular RNA circCTNNA1 promotes colorectal cancer progression by sponging miR-149-5p and regulating FOXM1 expression. Cell Death Dis. *11*, 557.

40. Yuan, D., and Zhu, Y. (2021). Knockdown of LINC01224 Suppresses Colon Cancer Progression by Sponging miR-485-5p to Downregulate MCL1. Cancer Manag. Res. *13*, 7803–7812.

41. Gu, J., Dong, L., Wang, Y., Nie, W., Liu, W., and Zhao, J.A. (2021). LINC01224 promotes colorectal cancer progression through targeting miR-485-5p/MYO6 axis. World J. Surg. Oncol. *19*, 281.

42. Clark, R.A., Qiao, J., Jacobson, J.C., and Chung, D.H. (2022). Induction of serine hydroxymethyltransferase 2 promotes tumorigenesis and metastasis in neuroblastoma. Oncotarget *13*, 32–45.

43. Liao, Y., Wang, F., Zhang, Y., Cai, H., Song, F., and Hou, J. (2021). Silencing SHMT2 inhibits the progression of tongue squamous cell carcinoma through cell cycle regulation. Cancer Cell Int. *21*, 220.

44. Jin, Y., Jung, S.N., Lim, M.A., Oh, C., Piao, Y., Kim, H.J., Nguyena, Q., Kang, Y.E., Chang, J.W., Won, H.R., and Koo, B.S. (2022). SHMT2 Induces Stemness and Progression of Head and Neck Cancer. Int. J. Mol. Sci. *23*, 9714.

45. Liu, C., Wang, L., Liu, X., Tan, Y., Tao, L., Xiao, Y., Deng, P., Wang, H., Deng, Q., Lin, Y., et al. (2021). Cytoplasmic SHMT2 drives the progression and metastasis of colorectal cancer by inhibiting beta-catenin degradation. Theranostics *11*, 2966–2986.

46. Pranzini, E., Pardella, E., Muccillo, L., Leo, A., Nesi, I., Santi, A., Parri, M., Zhang, T., Uribe, A.H., Lottini, T., et al. (2022). SHMT2-mediated mitochondrial serine metabolism drives 5-FU resistance by fueling nucleotide biosynthesis. Cell Rep. *40*, 111233.

47. Güllü, G., Karabulut, S., and Akkiprik, M. (2012). Functional roles and clinical values of insulin-like growth factor-binding protein-5 in different types of cancers. Chin. J. Cancer *31*, 266–280.

48. Shi, H., Liang, G.F., Li, Y., Li, J.H., Jing, A.H., Feng, W.P., Li, G.D., Du, J.X., and Feng, S.Y. (2019). Preparation and Evaluation of Upconversion Nanoparticles Based miRNA Delivery Carrier in Colon Cancer Mice Model. J. Biomed. Nanotechnol. *15*, 2240–2250.

49. Zhao, Y., Xu, J., Le, V.M., Gong, Q., Li, S., Gao, F., Ni, L., Liu, J., and Liang, X. (2019). EpCAM Aptamer-Functionalized Cationic Liposome-Based Nanoparticles Loaded with miR-139-5p for Targeted Therapy in Colorectal Cancer. Mol. Pharm. *16*, 4696–4710.

50. Juang, V., Chang, C.H., Wang, C.S., Wang, H.E., and Lo, Y.L. (2019). pH-Responsive PEG-Shedding and Targeting Peptide-Modified Nanoparticles for Dual-Delivery of Irinotecan and microRNA to Enhance Tumor-Specific Therapy. Small *15*, e1903296.

51. Pichler, M., Rodriguez-Aguayo, C., Nam, S.Y., Dragomir, M.P., Bayraktar, R., Anfossi, S., Knutsen, E., Ivan, C., Fuentes-Mattei, E., Lee, S.K., et al. (2020). Therapeutic potential of FLANC, a novel primate-specific long non-coding RNA in colorectal cancer. Gut *69*, 1818–1831.